Entropie : thermodynamique – énergie – environnement – économie
2026, vol. 7, n° spécial CIER, 16-30 pages, DOI : 10.21494/ISTE.OP.2026.1482 ISTE OpenScience

Uncovering Weakly Damped Nonlinear Inter-Aria Modes in High-RES Scenarios: A Koopman-Based Analysis of Tunisia's Future Grid

Mise en évidence des modes interzones non linéaires faiblement amortis dans des scénarios à forte pénétration renouvelable : Analyse basée sur Koopman du futur réseau électrique tunisien

Yassine BOUSSAA[1,2], Khadija BEN KILANI[3], Fethi GHODHBANE[4]

[1] Laboratoire des Systèmes électriques, ENIT, Université de Tunis El Manar,Tunis, Tunisie, yassine.boussaa@enit.utm.tn
[2] Ecole Supérieure Privée D'ingénierie et de Technologie, ESPRIT, Tunis, Tunisie, yassine.boussaa@esprit.tn
[3] Laboratoire des Systèmes électriques, ENIT, Université de Tunis El Manar,Tunis, Tunisie, khadija.kilani@enit.utm.tn
[4] Laboratoire des Systèmes électriques, ENIT, Université de Tunis El Manar,Tunis, Tunisie, fathi.ghodbane@enit.utm.tn

ABSTRACT. The increasing penetration of renewable energy sources (RES) significantly modifies power system dynamics by reducing inertia and amplifying nonlinear interactions. Conventional eigenvalue-based small-signal stability methods capture linearized behavior but fail to reveal hidden nonlinear oscillatory components emerging under renewable-rich conditions. This paper investigates the oscillatory stability of the Tunisian power grid projected for 2030 under a peak-load scenario with 35% RES penetration. Using a detailed nonlinear PSAT model, Classical Linear Modal Analysis (LMA) is combined with Koopman Modal Analysis (KMA), a data-driven operator-based approach extracting spatiotemporal dynamic structures from simulation data. Results show that LMA identifies the dominant inter-area mode near 0.8 Hz, while KMA reveals additional weakly damped nonlinear modes within the critical [0.7–1 Hz] band. Koopman mode shapes highlight a dominant North–[Centre + South] oscillation driven by the 400 kV transmission backbone, with time-domain reconstructions confirming long decay times. The study proposes targeted measures including PSS improvement, transmission reinforcement, PMU-based wide-area monitoring, and advanced control strategies. KMA is demonstrated as a powerful complement to classical modal analysis for future renewable-dominated grids.

RÉSUMÉ. L'intégration croissante des sources d'énergie renouvelables (SER) transforme profondément la dynamique des réseaux électriques en réduisant l'inertie et en amplifiant les interactions non linéaires. Cet article étudie la stabilité oscillatoire du réseau tunisien projeté à l'horizon 2030 dans un scénario de pointe nationale avec 35 % de SER, à travers une approche combinant l'analyse modale linéaire classique (LMA) et l'analyse modale de Koopman (KMA). Basée sur un modèle non linéaire développé sous PSAT, l'étude montre que la LMA identifie le mode interzone dominant autour de 0,8 Hz, tandis que la KMA révèle un spectre plus riche incluant des modes non linéaires faiblement amortis dans la bande critique [0,7–1 Hz]. Les formes modales de Koopman mettent en évidence une oscillation dominante Nord–[Centre+Sud] influencée par la structure du réseau 400 kV. Les résultats confirment des temps de décroissance élevés et soulignent la nécessité d'actions ciblées telles que l'amélioration des PSS, le renforcement du réseau, la surveillance PMU étendue et des stratégies modernes de contrôle. La KMA apparaît ainsi comme un outil complémentaire puissant pour l'analyse des futurs réseaux à forte pénétration renouvelable.

KEYWORDS. Inter-area oscillations, Koopman operator, DMD, non-linear modal analysis, large-scale renewable energy integration, Generators coherency, wide-area monitoring, Tunisian power system.

MOTS-CLÉS. Oscillations interzones, opérateur de Koopman, DMD, analyse modale non linéaire, intégration des énergies renouvelables, cohérence des générateurs, réseau électrique tunisien.

1. Introduction

The global transition toward low-carbon energy systems has accelerated the integration of renewable energy sources (RES), significantly modifying the structure and dynamics of modern power grids. The replacement of synchronous generators by converter-interfaced resources reduces system inertia, weakens electromechanical damping, and increases sensitivity to nonlinear interactions and operating-condition variations [MEZ 05], [BUD 12]. These challenges are particularly important in Tunisia, where wind and photovoltaic generation are expected to exceed 35% of the electricity mix by 2030, together with major reinforcements of the 225 kV and 400 kV transmission networks reshaping inter-area power exchanges between the North, Centre, and South regions.

Classical Linear Modal Analysis (LMA) is commonly used for small-signal stability assessment by extracting oscillation frequencies, damping ratios, and participation factors through system linearization [KUN 94]. However, its local nature limits its ability to represent nonlinear interactions and multi-frequency dynamics in high-RES systems.

To address these limitations, Koopman Modal Analysis (KMA) provides a data-driven framework capable of describing nonlinear dynamics without linearization. By projecting system dynamics into an observable space, the Koopman operator yields a linear representation of nonlinear evolution [BRU 22], while Dynamic Mode Decomposition (DMD) enables practical estimation of Koopman spectra from simulation or measurement data [SUS 11b], [TAK 17], [HAS 23].

In this work, KMA is applied to the Tunisian 2030 power system under a peak-load scenario with 35% RES penetration. A detailed nonlinear PSAT model including synchronous generators, combined-cycle units, converter-based renewable sources, and the updated 225/400 kV network is developed. Rotor speeds, rotor angles, and active powers are used to construct Hankel matrices and estimate Koopman spectra through DMD-based techniques.

The main contributions are: (i) a comparative LMA–KMA analysis revealing richer inter-area and nonlinear oscillatory behavior; (ii) identification of hidden nonlinear modes in the [0.7–1 Hz] range; (iii) coherency analysis combining geographical zoning and K-means clustering of Koopman modes; and (iv) stability enhancement recommendations including PSS tuning, network reinforcement, reactive compensation, and PMU-based wide-area monitoring. These results demonstrate the relevance of Koopman-based approaches for future low-inertia renewable-rich power systems.

2. Tunisian 2030 Grid and Simulation Framework

2.1. *System Modeling and Simulation Setup*

The Tunisian power system projected for 2030 undergoes significant structural changes, including reinforcement of the 225–400 kV transmission network, integration of new combined-cycle units, and large-scale deployment of renewable energy sources (RES). These modifications alter power-flow patterns, generation dispatch, and system inertia, strongly affecting overall dynamic behavior. To capture these effects, a detailed nonlinear model of the 2030 grid is developed using PSAT, based on an initial PSS®E network provided by STEG and updated according to national planning data.

2.2. *National Peak-Load Scenario in 2030 with 35% RES Penetration*

The system is organized around a meshed 225–400 kV backbone connecting three zones: the North (G1–G7, including Rades and BMC Zaghwen plants), the Centre (G10–G12, Sousse combined-cycle units), and the South (G13–G14, Gahnouch and Bouchemma units), as detailed in Table 1.

The study focuses on the peak-load condition (≈6000 MW), where 35% RES penetration increases North–Centre–South power transfers and stresses the transmission corridor, making the system more sensitive to inter-area oscillations. Fourteen synchronous generators are modeled using sixth-order representations with detailed excitation and turbine-governor dynamics. Wind and photovoltaic generation connected at 225 kV and 150 kV levels contribute to a 35% instantaneous renewable penetration level (IRPL), significantly reducing system inertia. A three-phase fault is applied at the Ezzahra 225 kV bus (cleared after 200 ms) to excite electromechanical dynamics, and nonlinear time-domain simulations are performed in PSAT over 20 seconds with a fine time step to capture both transient and sustained oscillatory behavior.

<table>
<tr><th></th><th>Category</th><th>Bus Number</th><th>Synchronous Generator Name</th><th>Abbreviated Name</th><th>P_{MAX} (MW)</th><th>Zone</th><th>Geographical Map</th></tr>
<tr><td rowspan="17">Synchronous Generators and Renewable Sources in the 2030 Peak Load Scenario (~6000 MW)</td><td rowspan="14">Conventional Sources (14 active synchronous generators)</td><td>343</td><td>TG RDC</td><td>G1</td><td>450</td><td rowspan="7">North</td><td rowspan="17">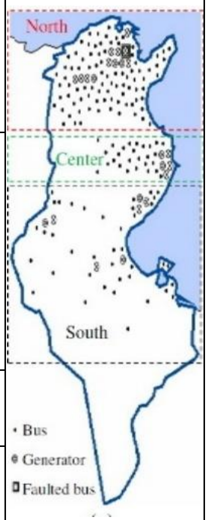
</td></tr>
<tr><td>344</td><td>TV RDC</td><td>G2</td><td>250</td></tr>
<tr><td>333</td><td>RADES2 G1</td><td>G3</td><td>150</td></tr>
<tr><td>335</td><td>RADES2 CC</td><td>G4</td><td>471</td></tr>
<tr><td>334</td><td>RADES2 G2</td><td>G5</td><td>150</td></tr>
<tr><td>345</td><td>BMC TG3</td><td>G6</td><td>120</td></tr>
<tr><td>346</td><td>BMC TG4</td><td>G7</td><td>120</td></tr>
<tr><td>326</td><td>TG CC1 SS</td><td>G8</td><td>120</td><td rowspan="5">Central</td></tr>
<tr><td>327</td><td>TG CC2 SS</td><td>G9</td><td>120</td></tr>
<tr><td>328</td><td>CC SS B</td><td>G10</td><td>424</td></tr>
<tr><td>340</td><td>CC_SS C</td><td>G11</td><td>424</td></tr>
<tr><td>341 (Slack Bus)</td><td>CC_SS D</td><td>G12</td><td>424</td></tr>
<tr><td>337</td><td>CC GHNCH</td><td>G13</td><td>412</td><td rowspan="2">South</td></tr>
<tr><td>352</td><td>TG3 BCHM</td><td>G14</td><td>240</td></tr>
<tr><td rowspan="2">Renewable Energy Sources IRPL :35%</td><td>Wind Power</td><td>Photovoltaic Power</td><td>Total (Wind + PV)</td><td></td><td></td></tr>
<tr><td>656,39</td><td>1469,66</td><td>2126,05</td><td></td><td></td></tr>
<tr><td colspan="4">Total Installed Capacity (Conventional + RES)</td><td colspan="2">6001MW</td></tr>
</table>

Table 1. *Geographical Distribution of Active Conventional and Renewable Generators in the 2030 Peak Load Scenario*

3. Methodology

This section presents the framework used to analyze the oscillatory behavior of the Tunisian 2030 power system. The proposed approach combines Classical Linear Modal Analysis (LMA), Koopman Modal Analysis (KMA), and coherency assessment using K-means clustering, providing complementary local and global insights into linear and nonlinear inter-area oscillations under high renewable penetration.

3.1. *Workflow of the Renewable Integration Study - Linear and Nonlinear Modal Analysis*

The study starts with a static power-flow analysis of the base network (without RES) using MATLAB/PSAT to establish steady-state operating conditions. Renewable generation is then gradually integrated by specifying injected power, technology type (PV or wind), converter structure, and control mode (P/V or P/Q). After each step, the operating point is updated and verified through power-flow convergence.

Dynamic analysis is performed using two complementary methods. LMA linearizes the system around the operating point to extract conventional eigenmodes, while KMA is directly applied to time-domain signals without linearization, capturing additional spectral content such as lightly damped modes, nonlinear interactions, and inter-area oscillations under varying operating conditions.

Finally, results from both approaches are compared to evaluate modal consistency and stability. If stability criteria are satisfied, the renewable penetration level is accepted; otherwise, injected power is adjusted until stability limits are met. Fig. 1 summarizes the overall workflow.

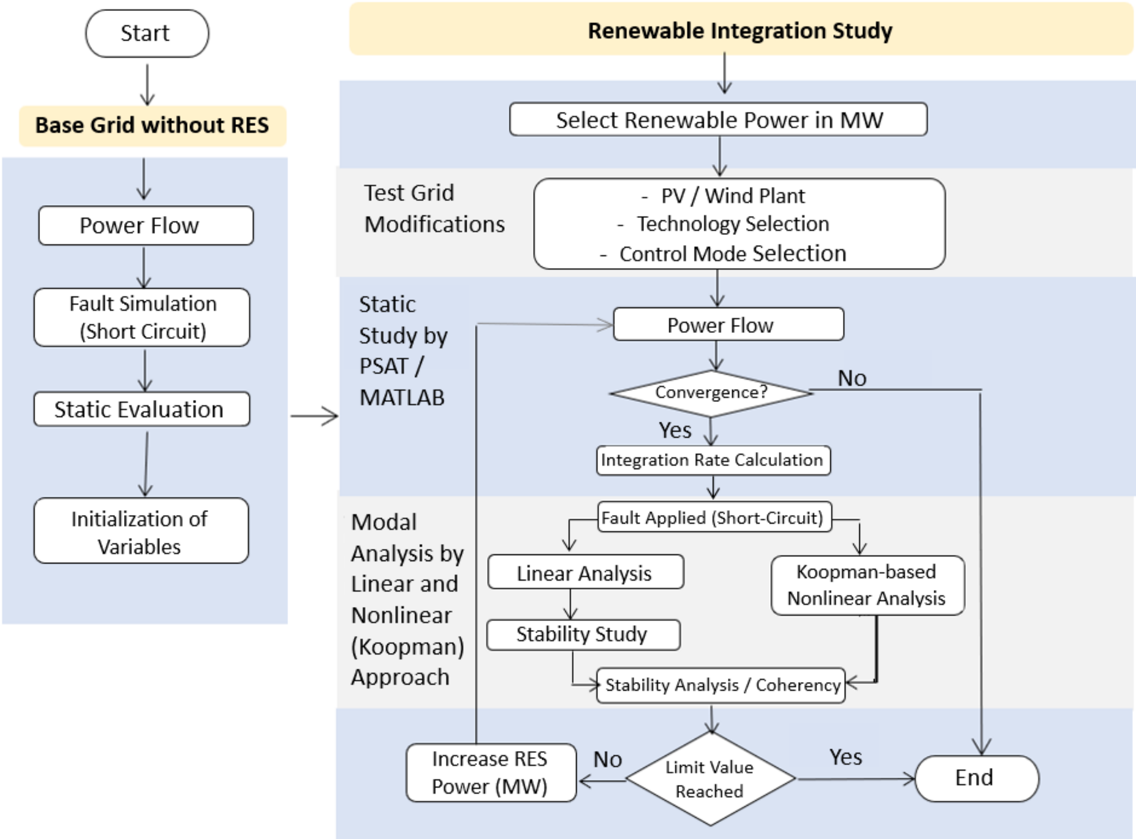

Figure 1. *Workflow of the Renewable Integration Study*

3.2. *The Koopman Operator Framework*

3.2.1. *Koopman Operator Definition*

Koopman Modal Analysis provides a powerful, data-driven framework rooted in operator theory. Instead of linearizing nonlinear equations, KMA lifts the system dynamics into a higher-dimensional space of observable functions, as in [SUS 11b]. In this space, the evolution of the system is governed by a linear Koopman operator.

The Koopman operator may be defined for the discrete-time autonomous nonlinear dynamical system, defined by the map in equation (1), evolving on a finite-dimensional manifold M,

$$xk + 1 = f(xk) \qquad [1]$$

where $x_k \in M$, k is an integer index and $f : M \rightarrow M$ denotes a map from the manifold M to itself, which describes the nonlinear state evolution. In addition, a scalar observable function $g : M \rightarrow R$ is given. Observable functions may be obtained from snapshots from numerical simulations or physical experiments, taken uniformly spaced in time. In a power system, observables denote dynamics of interest, such as generator swing dynamics, or voltages metered at pilot buses of the power grid. The Koopman operator U acts on this observable function as in (2), [SUS 11b][SUS 15]:

$$Ug(x) = (gof)(x) = g(f(x)) \qquad [2]$$

Therefore, the vector $\boldsymbol{g}(\boldsymbol{x}_k)$ measuring the observables at the discrete time k will be defined as follows:

$$\boldsymbol{g}(\boldsymbol{x}_k) = \sum_{j=1}^{\infty} U^k \varphi_j(\mathrm{x}_0) V_j = \sum_{j=1}^{\infty} \lambda_j{}^k \varphi_j(\mathrm{x}_0) V_j \qquad [3]$$

Observable snapshots are stacked in an observable matrix as in Fig. 2, and an Arnoldi-type algorithm is applied to approximate the point spectrum of the operator, confined in the empirical Ritz eigenvalues $\tilde{\lambda}_j$ and eigenvectors $\tilde{v}_j$.

3.2.2. *Point Spectrum Approximation*

While the modes capture correlations in components of the observable, the corresponding eigenvalues define growth/decay rates and oscillation frequencies for the mode. Nonetheless, the infinite dimensionality of the Koopman operator poses problem. This may be surpassed by truncating the operator to a finite subspace. This dimension reduction is accomplished by the dynamic mode decomposition procedure, which spectrum may be approximated by the empirical Ritz eigenvalues and eigenvectors noted respectively $\tilde{\lambda}_{\mathrm{j}}$ and $\tilde{v}_{\mathrm{j}}$.

Considering a sequence of $N+1$ observations $\{g(x_0), \cdots, g(x_N)\}$, and construct the data matrix X as in Fig. 2:

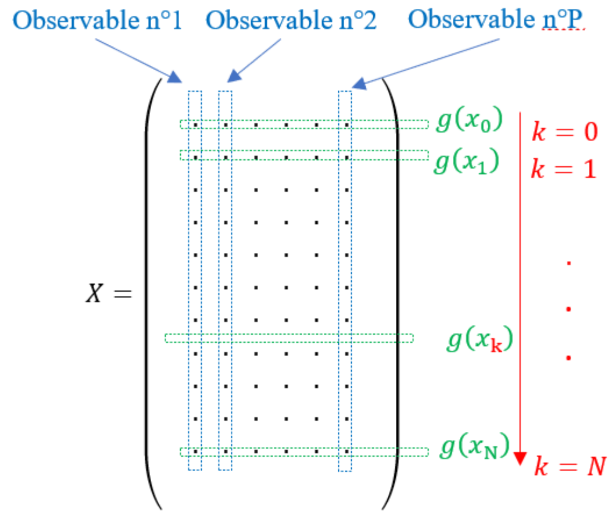

Figure 2. *Structure of the Observable Data Matrix Used for Koopman Analysis*

The Ritz eigenvalues are those of the companion matrix C defined by:

$$C = \begin{bmatrix} 0 & 0 & \dots & 0 & c_0 \\ 1 & 0 & \dots & 0 & c_1 \\ 0 & 1 & & 0 & c_2 \\ \vdots & & \ddots & & \vdots \\ 0 & 0 & \dots & 1 & c_{N-1} \end{bmatrix} = A^{\dagger}B, \qquad [4]$$

where $A = G^T \times G$; $B = G \times g(x_N)$; $G = [g(x_0), \dots, g(x_N - 1)]$; and $A^{\dagger}$: The Moore Penrose pseudoinverse of A. The Ritz eigenvectors $\tilde{v}_j$ which approximate the Koopman modes, correspond to the columns of V :

$$V = [g(x_0), \dots, g(x_N - 1)] \times T^{-1}, \qquad [5]$$

where T is the Vandermonde matrix defined as:

$$T = \begin{bmatrix} 1 & \tilde{\lambda}_1 & \tilde{\lambda}_1^2 & \cdots & \tilde{\lambda}_1^{N-1} \\ 1 & \tilde{\lambda}_2 & \tilde{\lambda}_2^2 & \cdots & \tilde{\lambda}_2^{N-1} \\ 1 & \tilde{\lambda}_3 & \tilde{\lambda}_3^2 & \cdots & \tilde{\lambda}_3^{N-1} \\ \vdots & \vdots & \vdots & \ddots & \vdots \\ 1 & \tilde{\lambda}_N & \tilde{\lambda}_N^2 & \cdots & \tilde{\lambda}_N^{N-1} \end{bmatrix}. \qquad [6]$$

Compared to (3), the empirical Ritz eigenvalues $\tilde{\lambda}_j$ and eigenvectors $\tilde{v}_j$ behave in the same manner as the Koopman eigenvalues and modes, but for the finite sum (7) instead of the infinite sum.

$$\begin{cases} g(x_k) = \sum_{j=1}^{N} \tilde{\lambda}_j^{\ k} \, \tilde{v}_j. & K = 0, \dots, N-1 \\ g(x_N) = \sum_{j=1}^{N} \tilde{\lambda}_j^{\ N} \, \tilde{v}_j + r & r = \{x_0, \dots, x_{N-1}\} \end{cases} \qquad [7]$$

The Koopman modes frequencies f_j are defined as:

$$f_j = \arg(\tilde{\lambda}_j) * f_s/2\pi \qquad [8]$$

where f_s is the sampling frequency and $\arg(\tilde{\lambda}_j)$ are the Koopman modes arguments defined by:

$$\arg(\tilde{\lambda}_j) = Im\ (\ln\ (\tilde{\lambda}_j))\ /\ 2\pi \qquad [9]$$

The main steps for the computation and selection of the Koopman point spectrum are summarized in Fig. 3.

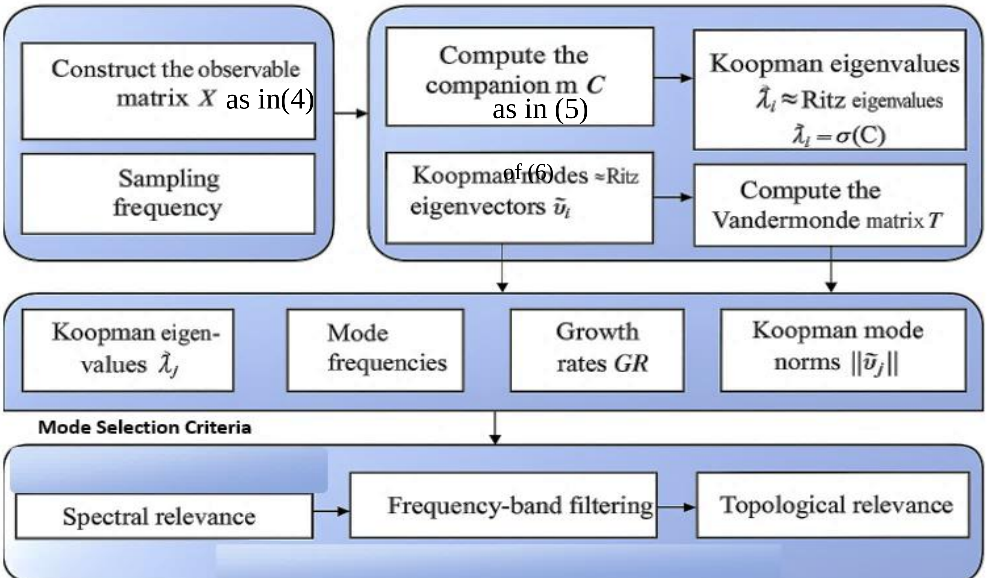

Figure 3. *Main steps for the computation and selection of the Koopman modes*

3.2.3. *Stability of Koopman Modes*

The performed Mode Decomposition not only provides dimensionality reduction in terms of a reduced set of modes but also sets a model for how these modes evolve in time. The damping ratio of Koopman modes are quantified by their growth rates. The growth rate GR_j of the j^{th} Koopman mode is determined by the amplitude of its j^{th} eigenvalue $\tilde{\lambda}_j$ [BRU 22], [JUA 22], [KUT 14], [TAK 20], [KUT 16].

$$GR_j = ln\ |\tilde{\lambda}_j|/\Delta t \qquad [10]$$

A smallest growth rate denotes a largest damping ratio. The stability limit of Koopman modes is defined by the unit circle as:

$$GR_j = ln\ |\tilde{\lambda}_j|/\Delta t = 1 \qquad [11]$$

An unstable Koopman eigenvalue has modulus larger than one. Its corresponding Koopman mode grows exponentially as time increases. A GR less than one involves a damped (stable) Koopman mode. For a given j^{th} Koopman mode, the temporal evolution of its growth rate is given by the j^{th} line of the matrix M, where each of its components M_{jk} is defined by the modulus of the component T_{jk} of the Vandermonde matrix T defined in equation (12):

$$M_{jk} = |T_{jk}| \qquad [12]$$

The modal vector (mode shape) $\mathbf{V}_j$, from which the norm $\| \mathbf{V}_j \|$is extracted, reflects the energetic contribution of the mode to the overall system behavior.

The damping ratio expressed in percentage is given by the following expression:

$$\zeta_{\text{damping}}(\%) = \frac{-\text{Re}\ ((\ln\ (\tilde{\lambda}_j))/\Delta t)}{|\ (\ln\ (\tilde{\lambda}_j))/\Delta t\ |} \times 100 \qquad [13]$$

It should be noted that the minimum damping ratio must remain above 5%.

The dominance criterion $D_k = GR_j \cdot \| \mathrm{V}_j \|$, which highlights modes that are simultaneously weakly damped and strongly represented in the system observables.

3.2.4. *Selection of Observables and Construction of the Hankel Matrix*

A key step in KMA is the selection of observables that capture the essential electromechanical behaviors of the grid. In this work, three categories of observables are used: Rotor speeds $\Omega_i(t)$, Rotor angles $\delta_i(t)$ and Active powers $P_{gen,i}(t)$.

These variables capture both linear and nonlinear contributions to generator dynamics and ensure accurate reconstruction of inter-area oscillatory patterns.

To embed temporal structure into the Koopman approximation, a Hankel matrix is constructed from time-shifted observable snapshots:

$$H = \begin{bmatrix} g(x_1) & g(x_2) & \cdots & g(x_m) \\ g(x_2) & g(x_3) & \cdots & g(x_{m+1}) \\ \vdots & \vdots & \ddots & \vdots \\ g(x_n) & g(x_{n+1}) & \cdots & g(x_{m+n}) \end{bmatrix} \qquad [14]$$

where $g(x_k)$contains all selected observables at time k.

This structured data matrix enables the extraction of dominant oscillatory components, capturing both transient and sustained behaviors activated during the fault. A sufficiently large number of delays ensures that both low- and high-frequency dynamics are preserved in the Koopman spectral estimate.

3.2.5. *Dynamic Mode Decomposition (DMD)*

The finite-dimensional approximation of the Koopman operator is obtained using Dynamic Mode Decomposition (DMD). DMD consists of:

- Performing singular value decomposition (SVD) to extract dominant temporal structures;
- Estimating a low-rank linear operator relating time-shifted snapshots;

- Extracting Koopman eigenvalues (frequencies, growth rates);
- Computing Koopman modes, representing the spatial oscillatory pattern for each mode.

Koopman eigenvalues take the form:

$$\tilde{\lambda}_j = e^{(\sigma_j + j\omega_j)\Delta t} \qquad [15]$$

where σ_j and ω_j represent growth/decay rates and oscillation frequencies, respectively. Koopman predominant modes represent the physically meaningful oscillatory structures driving system behavior. DMD is chosen for its robustness, computational efficiency, and proven ability to capture nonlinear oscillatory dynamics in power systems, as in [BRU 22], [JUA 22], [KUT 14].

3.2.6. *Filtering and Interpretation of Koopman Modes*

An essential part of DMD-based Koopman analysis is filtering trivial or spurious modes. The following criteria are used: Mode energy (dominance); Frequency band of interest (0.5–1.2 Hz); Spatial coherence across generators and Physical interpretability with respect to power flows and grid topology. This step isolates meaningful modes and avoids numerical artifacts.

3.3. *Generator Coherency Analysis Using Clustering*

Generator coherency is analyzed using two complementary approaches. First, a manual grouping based on the geographical structure of the Tunisian grid separates generators into three zones: North (G1–G7), Centre (G8–G12), and South (G13–G14), reflecting the main transmission corridors and historical operational boundaries. To complement this classification, a K-means clustering algorithm is applied to the complex Koopman mode shapes in order to automatically identify generators exhibiting similar oscillatory behavior in phase and amplitude. This data-driven approach provides an unbiased identification of coherent groups, validates and refines the geographical partition, and reveals hidden coherency patterns not directly observable from network topology alone. Three clusters are retained, consistently matching the North–Centre–South structure while providing improved dynamic insight..

3.4. *Summary of Methodological Advantages*

The combination of LMA, KMA, and data-driven clustering provides a multi-dimensional view of system stability:

- LMA identifies linear inter-area modes but cannot account for nonlinearities.
- KMA detects hidden nonlinear modes, long decay behaviors, and multi-frequency oscillations.
- Clustering reveals spatial coherency patterns essential for damping and control strategies.

This integrated methodology forms a robust foundation for the analysis of oscillatory stability presented in Section IV.

4. Results

This section presents the oscillatory analysis of the Tunisian 2030 power grid under the national peak-load scenario with 35% RES penetration. The results combine Classical Linear Modal Analysis (LMA), Koopman Modal Analysis (KMA), time-domain reconstruction, and generator coherency assessment to reveal both linear and nonlinear oscillatory structures.

4.1. *Linear Modal Analysis Results*

Linear Modal Analysis identifies three dominant inter-area modes within the frequency range 0.78–0.91 Hz, corresponding to North–Centre–South interactions in the Tunisian grid. The associated eigenvalues exhibit low damping ratios (3–6%), frequency clustering around 0.8–0.9 Hz, and strong participation from Northern generators (G2–G5).

Participation factor analysis confirms that the Rades synchronous units dominate the oscillatory dynamics. The Central combined-cycle units (G10–G12) participate moderately across all inter-area modes, whereas Southern units (G13–G14) show weaker but coherent participation.

Although LMA successfully identifies the dominant inter-area mode, its linear formulation remains limited to small perturbations and cannot capture nonlinear interactions or multi-frequency dynamics. This limitation motivates the use of Koopman Modal Analysis.

4.2. *Koopman Spectrum and Frequency Band Decomposition*

Koopman Modal Analysis reveals a significantly richer spectral structure than LMA. The selected observables include rotor speed (Ω), rotor angle (δ), and generator active power (P_{gen}). A Hankel matrix is constructed from the simulated trajectories, and the finite-dimensional Koopman operator is estimated using Dynamic Mode Decomposition (DMD) [KUT 16],[SAH 20].

The filtered Koopman spectrum within the [0–3 Hz] range, shown in Fig. 4, reveals four frequency regions: slow global dynamics below 0.5 Hz, inter-area oscillations between 0.5 and 1.1 Hz, mainly local dynamics between 1.1 and 2 Hz, and weak high-frequency components above 2 Hz. The most critical modes are concentrated within the [0.5–1.1 Hz] band, particularly between 0.76 and 0.96 Hz, where several modes exhibit damping ratios below 5%.

Among these modes, the KM-0.81 Hz mode is the most dominant and weakly damped, producing oscillations with decay times exceeding 10 seconds. This mode corresponds to an inter-area oscillation between the Northern region and the combined [Central + Southern] zones, representing the most critical dynamic interaction of the projected network and highlighting the need for dedicated damping strategies.

Fig. 5 illustrates the damping-ratio distribution of modes within the 0.01–1.2 Hz range. A critical zone is identified between 0.7 and 1.2 Hz, where several poorly damped modes may generate persistent oscillations following renewable fluctuations or network disturbances.

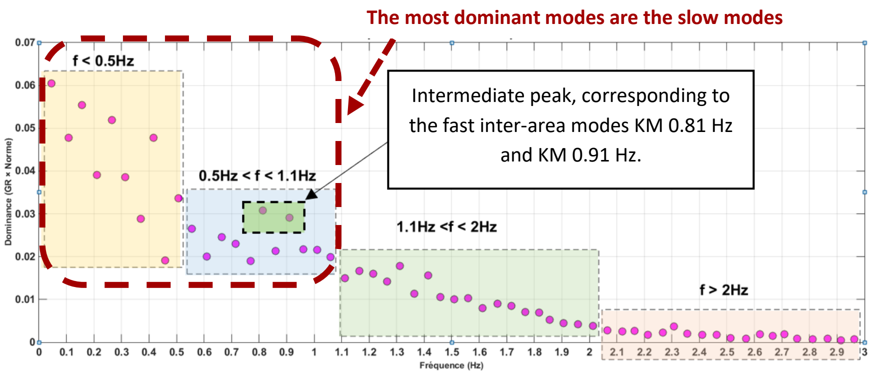

Figure 4. *Spectrum of the filtered Koopman modes in the [0–3 Hz] frequency band*

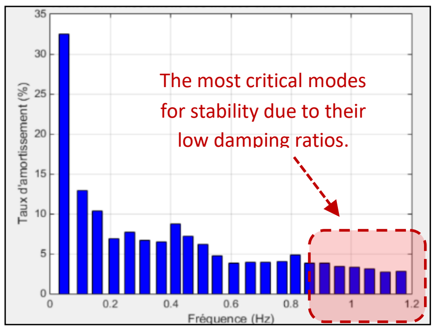

Figure 5: *Damping Ratios of Modes in the Inter-Area Oscillation Band*

Cross-referencing these results with the damping analysis and the mode-shape examination will help prioritize stability enhancement actions, particularly with regard to the network's most sensitive areas.

Generator coherence was analyzed using both manual geographic segmentation (North, Centre, South) and automated K-means clustering of complex modal vectors. Fourteen critical modes within the [0.5–1.2 Hz] band were classified into three topological groups. Fig. 6 illustrates the Koopman spectrum mapped in the frequency–dominance plane using *manual geographical grouping*, where each mode is represented according to its dominance.

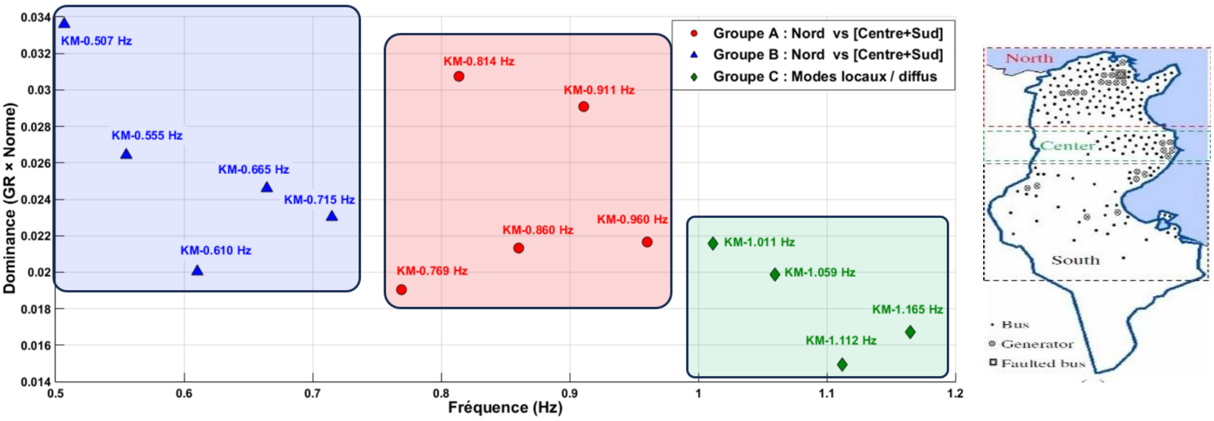

Figure 6. *Koopman spectrum in the frequency–dominance plane showing three topological groups*

Three topological groups emerge:

- Group A: (0.76–0.96 Hz) corresponds to well-structured inter-area oscillations, exhibiting clear North vs [Centre + South] dynamics, with strong participation of northern generators (G2–G5);
- Group B: (0.50–0.71 Hz) comprises moderately engaged inter-area modes where central combined-cycle units (G10–G12) act as stabilizing pivots;
- Group C: (>1 Hz) involves more localized or weakly structured oscillations confined to the Northern zone.

Table 2 provides the classification of Koopman modes into three topological groups based on their dominant characteristics and dynamic behavior.

The Mode Shapes associated with the dominant modes, shown in Fig. 7, confirm the existence of clear phase opposition between the Northern and Southern zones, characteristic of large-scale inter-area oscillations. These spatial patterns are consistent with the physical topology of the 400 kV backbone RADES–SIDI BOUZID–SKHIRA, which constitutes a weak coupling corridor under high renewable penetration. The oscillation pattern of the KM-0.81 Hz mode further emphasizes the need to strengthen this transmission path, particularly through reactive compensation and improved damping control.

When compared with classical linear modal analysis, KMA reproduces the main inter-area oscillation near 0.8 Hz but additionally exposes hidden nonlinear modes that are not detected in the small-signal framework. These hidden components reflect nonlinear energy exchanges among synchronous generators and converter-based renewable units, which become more significant in high-RES scenarios.

Group	Dominant Characteristics	Dynamic Behavior	Included Modes
A	Clear opposition between North vs. [Central + South], with strong involvement and high coherency of the Northern generators.	Well-structured inter-area modes, showing a distinct decoupling between G1–G7 (North) and G11–G12 (Central) + G13–G14 (South).	KM-0.813 Hz, KM-0.911 Hz, KM-0.961 Hz, KM-0.860 Hz, KM-0.768 Hz
B	Opposition between North vs. [Central + South], with a highly coherent but moderately involved Northern area.	Inter-area modes with strong participation of G2 and G4 (North), and weak involvement of Central and Southern generators. These modes are less structured but still engage all regions, with the Central area often weakly stressed or dynamically neutral.	KM-0.506 Hz, KM-0.554 Hz, KM-0.664 Hz, KM-0.715 Hz, KM-0.610 Hz
C	Weakly structured or local modes, dominated by a few generators in the Northern area.	Local or broad but weakly organized oscillations, typically centered on the Northern zone and characterized by internal detuning effects.	KM-1.112 Hz, KM-1.165 Hz, KM-1.059 Hz, KM-1.011 Hz

Table 2. *Topological Grouping of Koopman Modes in the Critical Frequency Band*

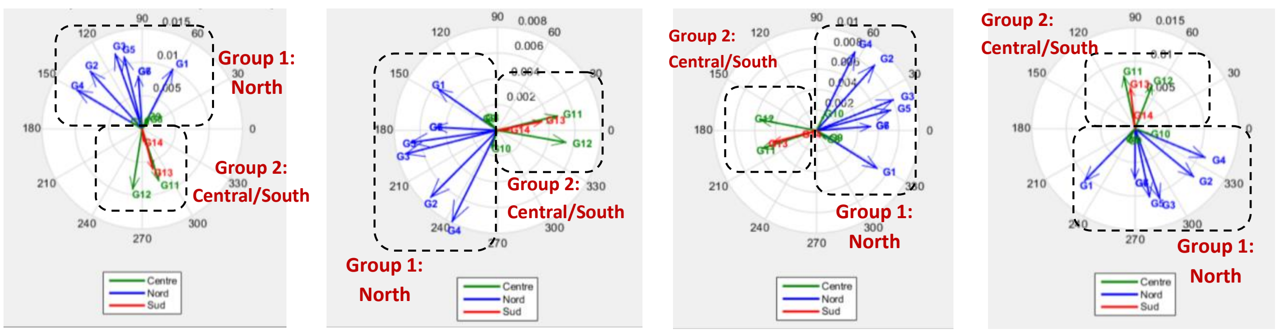

(KM-0.81Hz) The most dominant inter-area mode not captured by the AML

(KM-0.76Hz) Inter-area mode captured by AML and KMA

(KM-0.86Hz) Inter-area mode captured by AML and KMA

(KM-0.91Hz) Inter-area mode captured by AML and KMA

Figure 7. *Mode Shapes of the Most Dominant Koopman Modes - manually classified using geographical topology*

4.3. *Generator Coherency: Manual vs. Data-Driven Clustering*

The coherency structure of the Tunisian 2030 system is first analyzed using a manual geographical partition based on the grid topology, separating generators into three zones: North (G1–G7), Centre (G8–G12), and South (G13–G14). This decomposition reflects the historical structure of the network and provides an intuitive reference for interpreting inter-area oscillations.

A complementary data-driven analysis is then performed using K-means clustering applied to the Koopman mode shapes. This unsupervised approach automatically identifies three coherent groups that largely agree with the geographical zoning while providing a more detailed view of the underlying dynamic behavior. Cluster A (0.76–0.96 Hz) captures the dominant inter-area oscillations, characterized by strong interactions between the North and the rest of the system. Cluster B (0.50–0.71 Hz) corresponds to intermediate modes where the Central region plays a stabilizing role. Cluster C (above 1 Hz) is associated with mainly localized dynamics concentrated in the Northern area.

Overall, both the manual and data-driven approaches lead to consistent interpretations of system coherency. The Northern region appears as the main source of oscillatory activity, the Centre acts as a dynamic buffer between North and South, and the Southern region oscillates in a coherent manner with the Centre. These results are illustrated in Fig. 8, which shows the K-means clustering of Koopman modes, and Fig. 9, which presents the mode shapes in the critical [0.7–1 Hz] frequency band for each cluster.

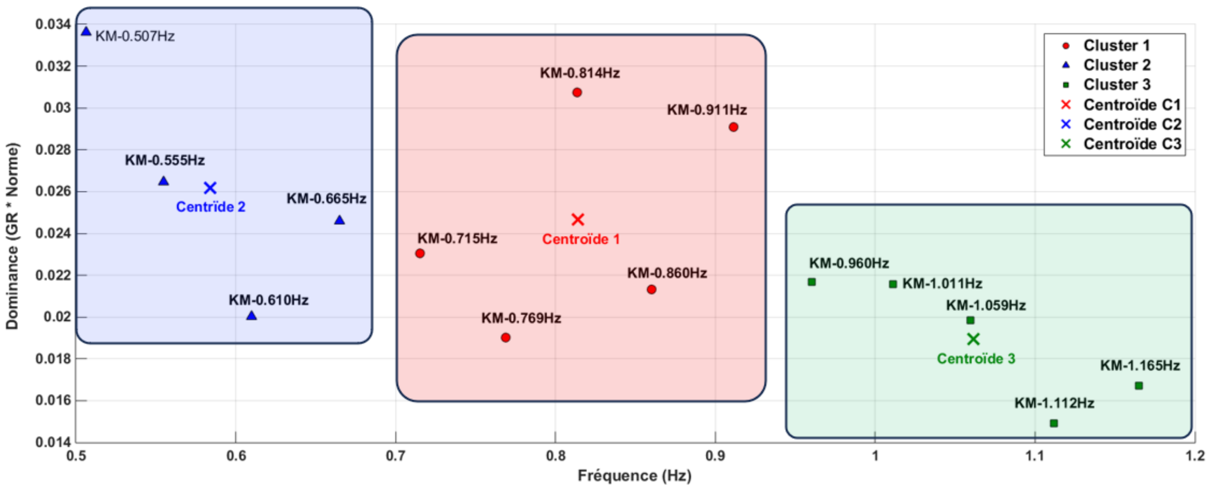

Figure 8. *Automatic K-means Clustering of Koopman Mode*

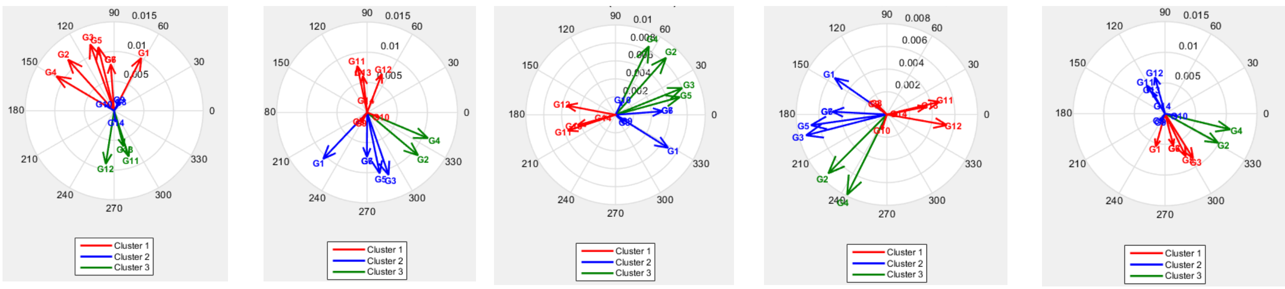

KM-0.814Hz KM-0.911Hz KM-0.860Hz KM-0.769 KM-0.715Hz

Figure 9. *Koopman mode shapes in the critical frequency band [0.7–1 Hz], automatically classified using K-means*

4.4. *Comparison Between Linear and Koopman Modal Analysis*

A direct comparison between the Linear Modal Analysis (LMA) and the Koopman Modal Analysis (KMA) reveals a strong agreement on the main oscillatory trends. Both methods identify the principal inter-area oscillation near 0.8 Hz, highlight the dominant involvement of Northern generators, and consistently show that the Centre and South tend to form a coherent dynamic block. These results confirm the reliability of the linear framework for capturing the primary oscillatory mode.

However, notable differences emerge when assessing richer or more complex dynamics. The Koopman approach uncovers nonlinear modes that remain invisible to LMA and provides a more accurate estimation of decay rates, whereas the linear model systematically underestimates them. KMA also offers a more detailed spatial interpretation through complex mode shapes, enabling the identification of multi-frequency oscillatory envelopes that LMA cannot resolve.

In summary, the Koopman analysis complements and significantly extends the capabilities of classical linear modal analysis, especially in networks with high renewable penetration where non-linear interactions become non-negligible.

5. Discussion

The oscillatory behavior of the Tunisian 2030 power system reveals important structural and nonlinear characteristics that become more pronounced under high renewable penetration. The combined use of Linear Modal Analysis (LMA) and Koopman Modal Analysis (KMA) provides complementary insights into these dynamics. At 35% renewable energy penetration, the reduction of synchronous generation leads to lower system inertia and weaker damping, while increasing the sensitivity of inter-area oscillations. In addition, KMA reveals hidden nonlinear modes in the 0.5–0.81 Hz range that are not captured by LMA, confirming the growing complexity of system dynamics under renewable-rich operating conditions. Both LMA and KMA consistently identify the North vs. [Centre + South] separation as the dominant inter-area oscillatory pattern, mainly due to the concentration of generation in the North and the stabilizing role of central combined-cycle units. The dominant mode around 0.81 Hz becomes more pronounced under stressed North–South power transfers, highlighting its critical role in system dynamics. KMA further shows that inter-area oscillations are not driven by a single mode but result from the interaction of several closely spaced modes, whose superposition produces amplitude modulation, slow decay, and multi-frequency behavior that cannot be captured by linear analysis. Coherency analysis using both geographical zoning and K-means clustering leads to a consistent interpretation of the system structure: the North acts as the main oscillatory source, the Centre behaves as a dynamic buffer, and the South remains coherently coupled with the Centre. K-means clustering further refines this structure by identifying subtle phase differences between generators, which is useful for control-oriented applications such as PSS tuning. Finally, LMA remains effective for identifying the dominant linear mode around 0.81 Hz and estimating small-signal stability, but it fails to capture nonlinear interactions and multi-modal envelopes. In contrast, KMA provides a richer spectral decomposition, more accurate damping estimation, and a clearer representation of coherency patterns. Together, both approaches offer a complete understanding of the system, where LMA captures the primary linear behavior while KMA explains the nonlinear and long-duration oscillatory phenomena. These results highlight that reduced inertia, weak damping, and corridor stress represent key vulnerabilities of the 2030 grid, requiring reinforcement, reactive power support, and advanced damping control strategies.

6. Recommendations for Stability Enhancement

The combined insights from LMA, KMA, time-domain simulations, and coherency analysis enable a set of targeted measures to enhance the oscillatory stability of the Tunisian 2030 grid under high renewable penetration, addressing both control-oriented and structural aspects of system performance. The Northern generators, particularly the Rades units (G2–G5) and the BMC Zaghwen turbines (G6–G7), exhibit the highest participation in the dominant 0.81 Hz mode and therefore provide the greatest leverage for damping improvement; priority should be given to Power System Stabilizer (PSS) installation or retuning on these units, with emphasis on the 0.7–1 Hz band where the main inter-area and nonlinear modes are concentrated, as this represents the most effective way to reduce system-wide oscillations. In parallel, the Centre (G10–G12), which acts as a dynamic buffer between North and South, should benefit from improved AVR/PSS coordination and, where possible, supplementary damping controllers to reinforce its stabilizing role and limit the propagation of oscillatory energy across the grid. Both LMA and KMA consistently highlight the structural vulnerability of the 225/400 kV North–Centre–South transmission corridor under high RES penetration, suggesting that its reinforcement through line uprating, additional transmission paths, enhanced reactive power support (SVC/STATCOM), and increased short-circuit strength in the South would significantly improve electromechanical stiffness and reduce inter-area coupling at its origin. Given the nonlinear and multi-modal oscillatory behavior revealed by KMA, real-time observability is also essential; therefore, the deployment of PMU-based wide-area measurement systems (WAMS) at key nodes such as Rades, Sousse, Gafsa, and Gabes, combined with online oscillation monitoring and wide-area damping control, would enable early detection of weakly damped modes and timely corrective actions as in [XIA 23]. Operational strategies can further complement structural measures by limiting persistent North–South power transfers, maintaining balanced inertia through optimized dispatch, incorporating dynamic security constraints into economic operation, and ensuring adequate spinning reserves, particularly in the Centre and South, thereby reducing oscillatory stress at low cost. In addition, the integration of grid-forming inverters represents a promising solution for future stability enhancement, as these devices can provide synthetic inertia and improve inter-area damping as in [WAN 22]; their pilot deployment in central and southern regions could significantly strengthen dynamic resilience. Overall, a prioritized implementation strategy emerges, combining reinforcement of PSS in the North, improved coordination of Central units, strengthening of the transmission corridor, deployment of WAMS, oscillation-aware operational adjustments, and gradual adoption of grid-forming technologies, forming a coherent pathway to address both linear and nonlinear stability challenges in the future low-inertia Tunisian grid, as in [BAZ 23].

7. Conclusion

This paper presented a comprehensive assessment of the oscillatory stability of the Tunisian power system projected for 2030 under a national peak-load scenario with 35% renewable energy penetration. By combining Classical Linear Modal Analysis (LMA), Koopman Modal Analysis (KMA), and data-driven coherency techniques, the study highlighted both linear and nonlinear dynamic mechanisms governing future grid behavior. LMA identified a dominant inter-area mode around 0.8 Hz driven by electromechanical interactions between generators in the North and those in the Centre and South. While effective for capturing the primary oscillatory behavior, LMA is limited by its linearization assumptions and cannot fully represent nonlinear effects, multi-frequency interactions, or long-duration transient dynamics typical of low-inertia systems. In contrast, KMA, derived from nonlinear time-domain simulations, revealed a richer modal structure with several weakly damped modes in the critical [0.7–1.0 Hz] range. The dominant Koopman mode at 0.814 Hz exhibited low damping and long decay times, consistent with LMA results but providing deeper insight into multi-modal interactions. Additional modes in the 0.55–0.81 Hz range exposed hidden nonlinear dynamics absent from the linear spectrum, underscoring the limitations of classical small-signal analysis in renewable-dominated grids. Spatially, Koopman mode shapes revealed a clear coherency pattern, with the North acting as the main oscillatory region, the Centre functioning as a stabilizing buffer, and the South oscillating coherently with the Centre. The agreement between geographical coherency analysis and K-means clustering of Koopman modes confirms the robustness of these structural patterns and highlights the influence of network topology and reduced inertia due to renewable integration. Overall, the combined spectral, spatial, and time-domain analyses emphasize the need for targeted damping actions, including PSS tuning in Northern units, improved coordination of central combined-cycle plants, reinforcement of the 400 kV North–Centre–South corridor, and deployment of PMU-based wide-area monitoring systems. The integration of grid-forming inverters is also identified as a promising solution for enhancing dynamic stability under high renewable penetration. This work demonstrates that Koopman Modal Analysis is a powerful complement to classical methods, providing deeper insight into nonlinear dynamics, hidden oscillatory modes, and coherency structures. As the Tunisian grid evolves toward higher renewable penetration, operator-theoretic and data-driven approaches will become essential for ensuring secure and resilient system operation. Future work will focus on real PMU-based Koopman monitoring, adaptive damping control strategies, and the impact of inverter-based resources on real-time stability.

Acknowledgment

The authors are grateful to Electrical Systems Laboratory of the National Engineering school of Tunis (ENIT) for supporting this work and providing the facilities needed to achieve this paper.

References

[BAZ 23] BAZRAFSHAN M., GIBBARD M., « Inter-area oscillations in low-inertia grids », *IEEE Transactions on Power Systems*, 2023.

[BRU 22] BRUNTON S. L. et al., *Koopman Operator Theory for Dynamical Systems*, Cambridge University Press, 2022.

[BUD 12] BUDISIĆ M., MOHR R., MEZIĆ I., « Applied Koopmanism », *Chaos*, vol. 22, n° 4, article 047510, 2012.

[HAS 23] HASSAN S. et al., « Koopman-based modal analysis for renewable systems », *IEEE Access*, vol. 11, 2023.

[JUA 22] JU L., ZHU H., « Generator coherency from data-driven mode shapes », *IEEE Transactions on Power Systems*, vol. 37, n° 2, 2022.

[KUN 94] KUNDUR P. et al., *Power System Stability and Control*, McGraw-Hill, 1994.

[KUT 14] KUTZ J. N., ROWLEY C. W., PROCTOR J. L., « Dynamic Mode Decomposition », *Journal of Computational Dynamics*, vol. 1, n° 2, 2014.

[KUT 16] KUTZ J. N., BRUNTON S. L., BRUNTON B. W., PROCTOR J. L., *Dynamic Mode Decomposition: Data-Driven Modeling of Complex Systems*, SIAM, 2016.

[MEZ 05] MEZIĆ I., « Spectral properties of dynamical systems, model reduction and decompositions », *Nonlinear Dynamics*, vol. 41, p. 309-325, 2005.

[SAH 20] SAHA S., CHOWDHURY B. H., « Dynamic modeling of renewable-integrated power systems using Koopman operator theory », *Electric Power Systems Research*, vol. 189, article 106750, 2020.

[SUS 11a] SUSUKI Y., MEZIĆ I., HIKIHARA T., « Coherent swing instability of power grids », *Journal of Nonlinear Science*, vol. 21, n° 3, p. 403-439, 2011.

[SUS 11b] SUSUKI T., MEZIĆ I., « Nonlinear Koopman modes and coherency identification », *IEEE Transactions on Power Systems*, vol. 26, n° 4, p. 1890-1901, 2011.

[SUS 15] SUSUKI Y., MEZIĆ I., « Nonlinear Koopman modes and coherency identification of coupled swing dynamics », *IEEE Transactions on Power Systems*, vol. 31, n° 2, p. 1191-1200, 2015.

[TAK 17] TAKEISHI N., KAWAHARA Y., « Learning Koopman invariant subspaces », *Advances in Neural Information Processing Systems (NeurIPS)*, 2017.

[TAK 20] TAKEISHI N., KAWAHARA Y., « Data-Driven Spectral Analysis of Nonlinear Power System Dynamics Using Koopman Operators », *Electric Power Systems Research*, vol. 189, article 106708, 2020.

[TAN 17] TANTET A., VAN DER WEG W., DIJKSTRA H. A., « Application of Koopman mode decomposition to the large-scale dynamics of electrical power grids », *Chaos*, vol. 27, n° 9, article 093110, 2017.

[WAN 22] WANG Z. et al., « Grid-forming inverters for oscillation damping », *IEEE Transactions on Energy Conversion*, vol. 37, n° 4, 2022.

[XIA 23] XIA T., ANDERSSON G., « Wide-area damping in renewable grids », *Electric Power Systems Research*, vol. 211, 2023.

